# SEISMIC BEHAVIOUR OF DRY STONE RETAINING WALLS: EXPERIMENTAL AND NUMERICAL PSEUDO-STATIC STUDIES

Nathanaël Savalle, Eric Vincens, Stéphane Hans

# SEISMIC BEHAVIOUR OF DRY STONE RETAINING WALLS: EXPERIMENTAL AND NUMERICAL PSEUDO-STATIC STUDIES

**Conference Paper** · July 2018

CITATIONS
3

READS
537

**3 authors:**

Nathanaël Savalle
Université Clermont Auvergne
**25** PUBLICATIONS **119** CITATIONS
SEE PROFILE

Eric Vincens
Ecole Centrale de Lyon
**71** PUBLICATIONS **924** CITATIONS
SEE PROFILE

Stéphane Hans
Ecole Nationale des Travaux Publics de l'Etat
**70** PUBLICATIONS **1,450** CITATIONS
SEE PROFILE

10th IMC
10th International Masonry Conference
G. Milani, A. Taliercio and S. Garrity (eds.)
Milan, Italy, July 9-11, 2018

# SEISMIC BEHAVIOUR OF DRY STONE RETAINING WALLS: EXPERIMENTAL AND NUMERICAL PSEUDO-STATIC STUDIES

**N. SAVALLE[1], E. VINCENS[1], S. HANS[2]**

[1] University of Lyon, LTDS, UMR CNRS 5513, Ecole Centrale de Lyon, Ecully, France
36 Avenue Guy de Collongue 69134 Ecully Cedex
e-mail: nathanael.savalle@ec-lyon.fr eric.vincens@ec-lyon.fr

[2] University of Lyon, LTDS, UMR CNRS 5513, Ecole Nationale des Travaux Publics de l'Etat, Vaulx-en-Velin, France
3 rue Maurice Audin 69518 Vaulx-en-Velin Cedex
e-mail : stephane.hans@entpe.fr

**Keywords:** Seismic, Scaled-down experiments, Dry stone, Masonry, Earthquake, DEM

**Abstract.** *Dry stone retaining walls (DSRWs) are vernacular structures, present worldwide, and made of rubble stones assembled with a precise know-how without any mortar. As many of them were built in the XIX$^{th}$ century and have not been maintained for decades, they need today some repairs or even sometimes whole reconstruction. However, the lack of national or international standards for the dry stone construction makes these necessities difficult to achieve. Recent researches have given a step forward into the understanding of the static behaviour of DSRWs. But since many of these DSRWs are built in seismic areas, there is a need for seismic recommendations. This work intends to provide some clues in this respect. A pseudo-static analysis has been first carried out as recommended by the Eurocode 8. First, some experiments were performed where a scaled-down wall retaining a backfill was tilted until failure. The results have been used to validate a numerical model based on a mixed continuum-discrete approach. The tilting angle of the mock-up at failure found by the simulations was found very close to the one obtained through the experiments. It validates this code for studying the behaviour of DSRWs by a pseudo-static approach, the next step will involve a validation for carrying out dynamic investigations on DSRWs.*

## 1 INTRODUCTION

Dry stone retaining walls are vernacular structures that can be found all over the world. These structures are used to build agricultural terraces and roads in mountainous areas. They have so shaped some regions that today some iconic sites are included in the UNESCO world heritage patrimony (Douro's valley, Portugal, Lavaux's terraces, Switzerland).

These walls are made of local stones assembled together without mortar. The friction between blocks and their weight strongly contribute to the stability of the structure. Moreover, each block, and even the smallest one, is put manually and carefully by the mason. Particularly, each joint (between two stones) of one layer should be overlapped by a stone from the upper layer, creating a staggered system. This overlapping gives an overall "bond strength" to the wall and ensures its stability.

Today, there are still numerous dry stone retaining walls (DSRWs) in many regions of the world. Particularly, in France, these structures are often very old and have been built in the end of the nineteenth century. Because of a lack of maintenance, this heritage is highly damaged and need today huge repairs.

There are many motivations to repair these structures with the same construction technique. Among them, we can mention the cultural heritage with the underlying tourist economy, the low amount of energy used for the construction, the reusability and recyclability of stones and the natural porosity of these walls that made them very useful in a water-flow environment. However these rehabilitations are difficult to achieve because of a lack of national and international guidance.

It explains the revival of scientific studies that have been carried out for twenty years in order to characterise the behaviour of DSRWs. Full-scale experiments have been carried out to understand the mechanisms of failure of these walls [1, 2, 3] and have been used to validate analytical models. Villemus used a limit-equilibrium method, validated on tests where walls were loaded by a hydrostatic charge. Colas validated an analytical method based on the yield design and homogenization on full-scale tests where the walls were loaded by a backfill made of gravel. Other analytical models have been developed to assess the stability of DSRWs [4, 5, 6]. Additionaly, numerical investigations have been performed [7, 8, 9]. Even if their predictive potential is not higher than analytical models, they can be used to understand the mechanisms of failure more in detail or to run case studies.

To complement these studies, cases where DSRWs retaining a backfill loaded by a concentrated load were investigated more recently by several authors [10, 11]. This concentrated load can model the presence of a vehicle on a road retained by the wall.

However, the seismic behaviour of DSRWs has not been investigated yet. Today, design methods of civil engineering structures take into account this risk. Unfortunately, they are not adapted to the specificities of dry stone construction. Indeed, in dry stone construction, blocks can move within the wall without triggering failure. Moreover, static studies have already pointed out that the failure surface can cross the structure in dry stone construction which is not the case in conventional technologies.

The Eurocode 8 [12] gathers the guidance for the seismic design of civil engineering structures. Particularly, the pseudo-static approach based on the Mononobe-Okabe method is the first (and simplified) method recommended to study the behaviour of retaining walls in seismic areas [13, 14]. It arises from the ease to carry out analytical developments with such an approach. Furthermore, it does particularly fit the engineering design due to fast computations. However, the pseudo-static approach is known to become over-conservative as the seismic acceleration increases [15]. To this extent, numerical models which are more sophisticated

(than analytical ones) can bring some clues to improve this simplified approach by studying the failure mechanisms and to point out their limits.

In this paper, scaled-down experiments have been conducted where a mock-up of a wall retaining a backfill made of sand was tilted. Then, a numerical model based on UDEC code (ITASCA) [16] has been validated on the basis of the experiments. Finally, some perspectives are given concerning the study of the seismic behaviour of DSRWs.

## 2 EXPERIMENTAL PROTOCOL

### 2.1 Principle of the test

The studied wall-soil system was composed of a retaining wall made of clay bricks retaining a backfill made of Hostun sand. The wall-soil system was installed in a container that was tilted until failure of the wall (Figure 1). As the mock-up was inclined, the natural gravity can be decomposed into two components (Figure 2): $a_h$, perpendicular to the wall which is the pseudo-static action that models the inertial forces due to the horizontal seismic motion and $a_v$, parallel to the wall. The tilting angle of the mock-up at wall failure was reported and the tests were filmed to analyze the mechanism of failure.

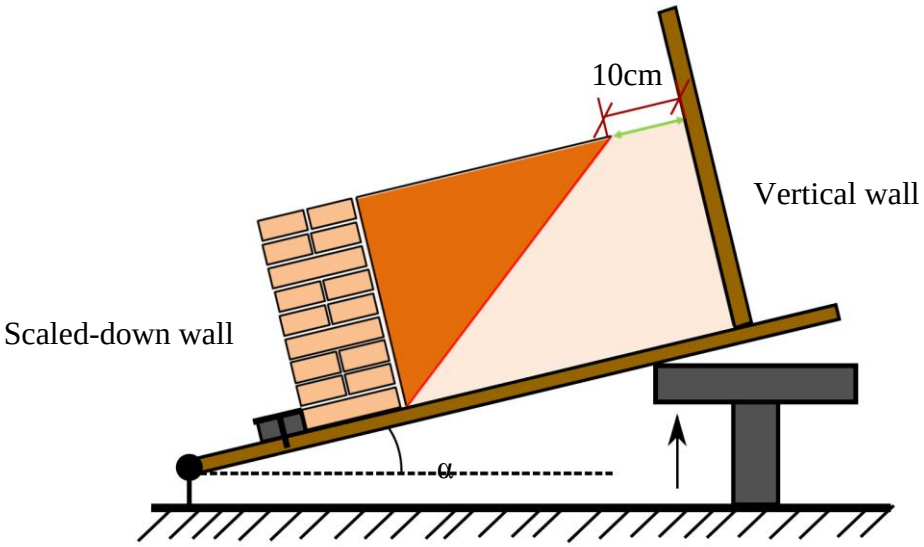


Figure 1: The container with the wall-soil system is tilted by a plunge until the wall failure. A small piece of wood at the wall toe prevents any translational movement of the first layer of bricks.

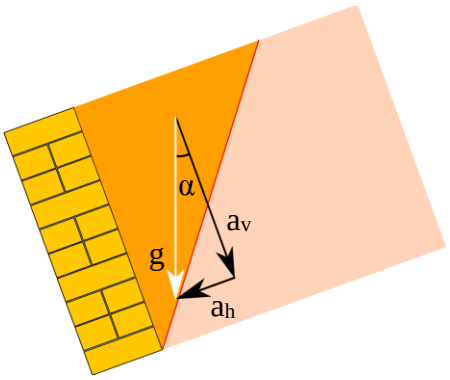


Figure 2: The natural gravity is decomposed into two components during the titling of the mock-up.

## 2.2 Devices and material used

The container in which the wall and the backfill have been placed had dimensions of (length*width*height = 40cm*40cm*25cm) (Figure 3). The width of 40cm ensured that the failure within the backfill cannot reach the rear vertical wall of the container (Figure 1). The wall made of clay bricks was placed in the aperture of the container. Its variable length (L) allowed the study of the impact of the length of the wall on the tests. It varied from 10cm to 40cm. The width of the wall (B) was constant through all experiments and equal to 34mm. The height of the wall (H) varied from 50mm to 150mm to investigate the influence of the slenderness (H/B) on the experiments. The backfill was made of Hostun sand that has been progressively deposited from a zero drop height in the container to obtain a very loose state for the material. The whole system was then tilted using a plunge (Figure 1).

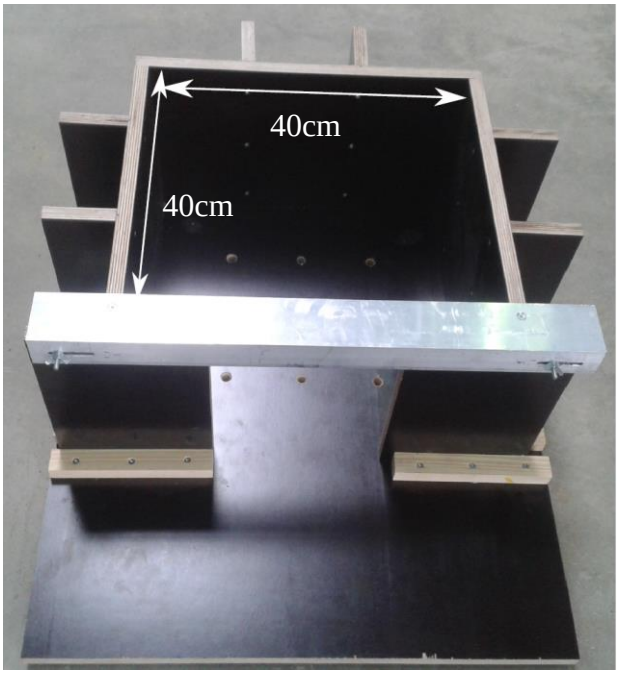


Figure 3: Container for the experimental tests. The wall is placed in the aperture which is variable (maximum length: 40cm).

To clarify the boundary condition in the backfill in contact with floor of the container, some sand grains have been glued to the floor of the container to impose the friction. Concerning the wall, a piece of wood prevented any translational movement of the first row of bricks (Figure 1) to model the foundation in actual DSRWs and to avoid to consider the friction between the bottom of the wall and the container which was unknown. Finally, the sides of the wall were not in contact with the container to prevent any restrictions of movement. A piece of deformable plastic was placed in the resulting space in order to avoid the seepage of the sand.

## 2.3 Characteristics of the materials

The clay bricks constituting the wall had dimensions of h*l*b = 11mm*17mm*34mm. The friction between bricks has been evaluated by Quezada [11] to 32° (±2°). Their unit weight was 16.2kN/m$^3$ (±0.05kN/m$^3$). However, the unit weight of the wall is lower due to the porosity: 14.4kN/m$^3$ (±0.27kN/m$^3$). The unit weight of the sand has been found to be equal to

13.2kN/m$^3$ (±0.45kN/m$^3$) in the experiments. It corresponds to a relative density of $R_D$ = 4%. The friction angle of this loose sand has been drawn from the work of Quezada et al. [11] who used a similar set-up. Other information for Hostun sand can be found in the work of Flavigny et al [17].

The behaviour of the interface between the wall and the backfill has been investigated in this study. In fact, although in the case of actual DSRWs the relative roughness of blocks can lead to consider that the friction angle of the interface is equal to the friction angle of the backfill, such considerations do not apply in the case of the regular bricks used in this work. To identify the friction of the wall-sand interface, fifteen bricks were glued together following the assemblage used for the wall and placed on a 70mm high layer of sand. The system was tilted until a slide of the glued blocks occurred. The tilting angle was reported. By means of eighteen tests, the friction of the interface has been evaluated to 22.7° (±2°).

## 3 EXPERIMENTAL RESULTS

### 3.1 Preliminary tests

#### *3.1.1. Study of the assemblage*

As the arrangement of stones is described in many books devoted to the building of DSRWs, the influence of the arrangement on the results has been first investigated. In particular, the importance of the presence of headers was studied (Figure 4). In the experiments, the geometry of the clay bricks allowed us to study three arrangements (Figure 5).

Figure 4: Top view of an assemblage studied in the experiments. Stretchers (light color) and headers (dark color) are presents

Case (b) is the only one which is consistent with the standards of the dry stone construction where all the layers are created with staggered patterns. Indeed, in the other two cases, many vertical joints are uninterrupted. For each arrangement, two scaled-down wall of dimensions (B = 34mm, H = 100mm, L = 200mm) have been erected, backfilled by sand and then tilted. It has been first observed that case (a) and (c) have failed partially. It means that only a part of walls fell whereas another one remained stable. In fact, due to the uninterrupted joints, the different parts of the wall are not linked and can behave separately. In actual DSRWs, this pattern is to be avoided because the loads and the materials are not so homogenous than in idealised experiments: weaknesses of the wall have to be balanced by its strengths and so all parts of the wall have to be linked to enable this scheme.

Case (a) was the one for which the tilting angle at failure was the higher (10.3° and 10.6°), followed by case (b) (8.5° and 9.1°) and by case (c) (2.6° and 3.1°). It emphasises that a construction with only headers in actual DSRWs would provide the more efficient arrangement for the resistance of the wall. However, it is often very difficult, depending on the kind of material used to find long blocks in a sufficient number; moreover, such headers in thick walls are too heavy to be easily processed. Then, it is only commonly advised to place the more headers as possible in the wall, as long as it does not lead to uninterrupted vertical joints. Thus, actual assemblages of DSRWs are close to the idealised one presented in case (b). Case

(c) is the less resistance arrangement and is the arrangement used by non-expert masons. This latter assemblage is typical in conventional masonry using mortar.

All the next experimental walls were erected using arrangement (b). Some double blocks (two headers glued together) have been used on the side of the scaled-down walls (Figure 4).

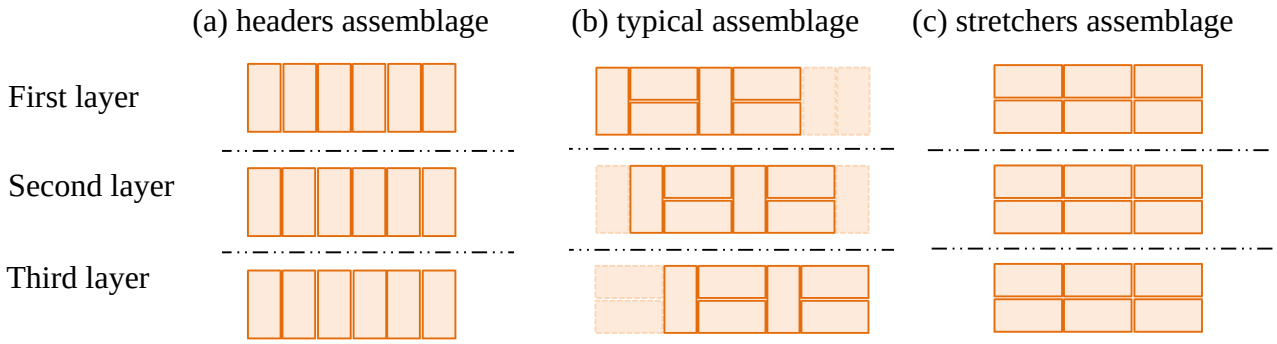


Figure 5: Top view of three different assemblages with headers and stretchers. (a) An assemblage using only headers. (b) A typical assemblage respecting the standards of dry stone construction. (c) An assemblage using only stretchers.

### *3.1.2. Plane deformation of the mock-up*

This experiments data set aims at validating the plane deformation mode for the wall failure. As the length of the wall is variable, four walls of similar height (H) and width (B) but with different lengths were built in the container, backfilled and then tilted to see the influence of the length of the wall on the tilting angle at failure and on the failure pattern. The results shown in Figure 6 indicate that although five tests have been done for each length no general trends can be deduced.

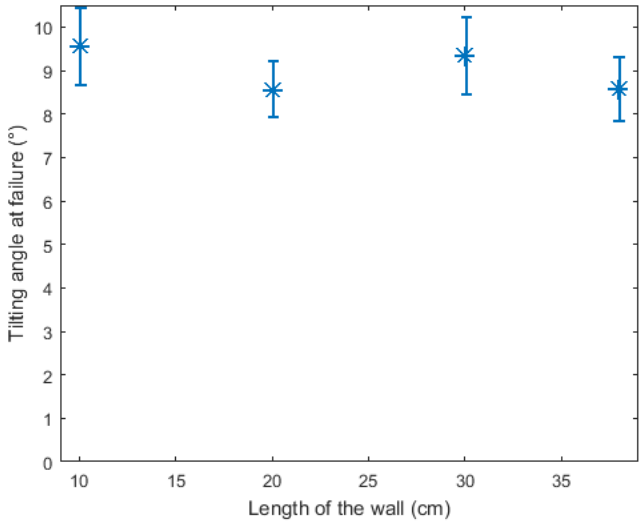


Figure 6: Influence of the length of the wall on the tilting angle at failure. No clear influence is observed.

Two particular tests have been filmed precisely. The first one corresponded to a wall of full length (L = 40cm) and the second to a wall of lower length (L = 20cm). Figure 7 shows a top view of the backfill at the moment of failure. In the first case (full length), the failure curve is

fairly a straight line (blue line in Figure 7) whereas in the second case, the failure curve is not a straight line. Consequently, length L is taken equal to 40cm for the subsequent tests.

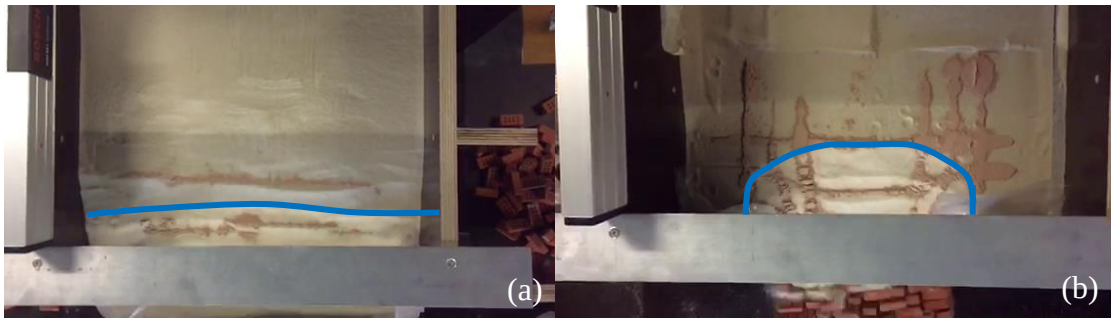


Figure 7: Top view of the failure of two walls of different lengths. (a) Straight failure line. (b) Failure curve.

### *3.1.3. Arching effect of the wall*

It has been mentioned in the previous section that the brick walls were not in contact with the lateral walls of the container to prevent from any arching effects in the wall that would lead to over-estimate its resistance. The influence of the value of the space, denoted Δ, on the tilting angle of the mockup has been investigated. Δ varied from 0mm to 35mm. Figure 8 presents the results and one can note that as long as the space Δ is not null, it seems to have no influence on the results. For experimental convenience, Δ was taken equal to 8mm.

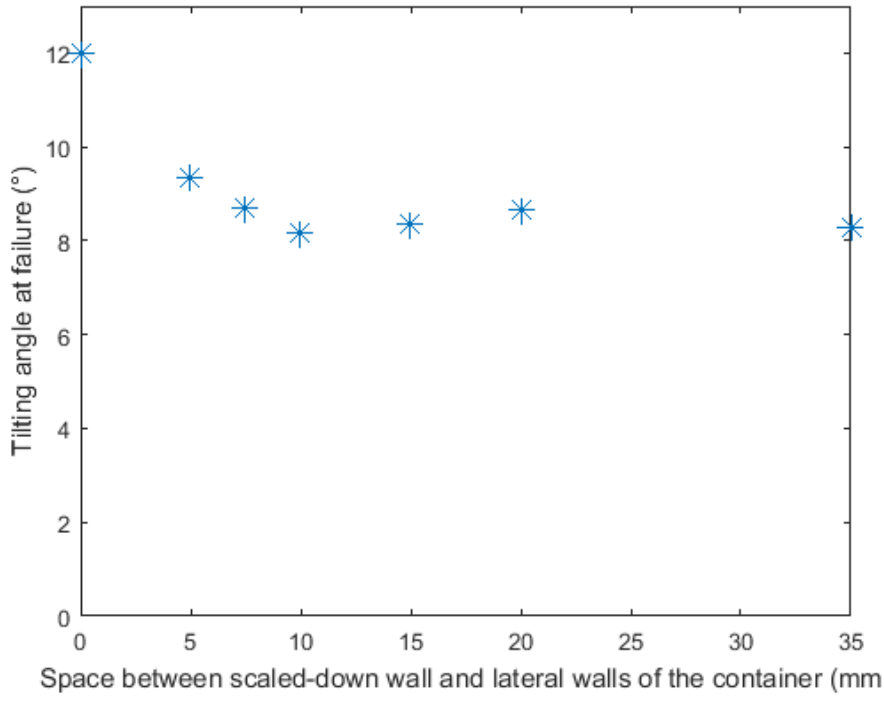


Figure 8: Influence of the space Δ between scaled-down wall and container's walls on the tilting angle at failure. The space Δ is present on both sides of the wall.

### *3.1.4. Repeatability tests*

Last but not least, some repeatability tests have been carried out to ensure the quality of the results. For four different walls with different slendernesses (H/B = 1.3; H/B = 2.7; H/B = 3.3;

H/B = 3.7), six identical tests have been conducted. Some departure can arise from the construction of the brick wall or from the installation of the backfill. In addition, small heterogeneities of the materials can lead to some disparities. The standard deviation for each of the four studied walls has been found smaller than 1°. This dispersion will be used to analyse the further tests.

### 3.2 Influence of the geometry of the wall

The influence of the geometry of the retaining wall on the tilting angle at failure is studied. Ten scaled-down walls with a same width B = 34mm and different heights H are backfilled with the loose sand. The mock-up is tilted and the angle of inclination of the container at failure is reported. Figure 9 presents the experimental tilting angles found in function of the slenderness (H/B) of the wall. The results of the repeatability tests are also depicted in this figure. As expected, the more slender the wall, the lower the tilting angle is obtained. Moreover, the two typical modes of failure of DSRWs have been observed: toppling (Figure 10) and sliding (Figure 11). The toppling mode of failure occurs for more slender walls whereas sliding occurs for the less slender ones.

In these two modes of failure, the wall was cut into two sub-systems by the failure surface. One part of the wall fell down and the other one remained stable and stayed in place. In the sliding mode of failure, this failure surface was found to be horizontal separating the first row of bricks (whose translational movement was prevented) from the top rest of the wall. In the toppling mode of failure, the failure surface is oriented by an angle of around 11° with the horizontal. The first layer of bricks and some bricks of the inner face of the second row of the brick walls remained stable (Figure 12).

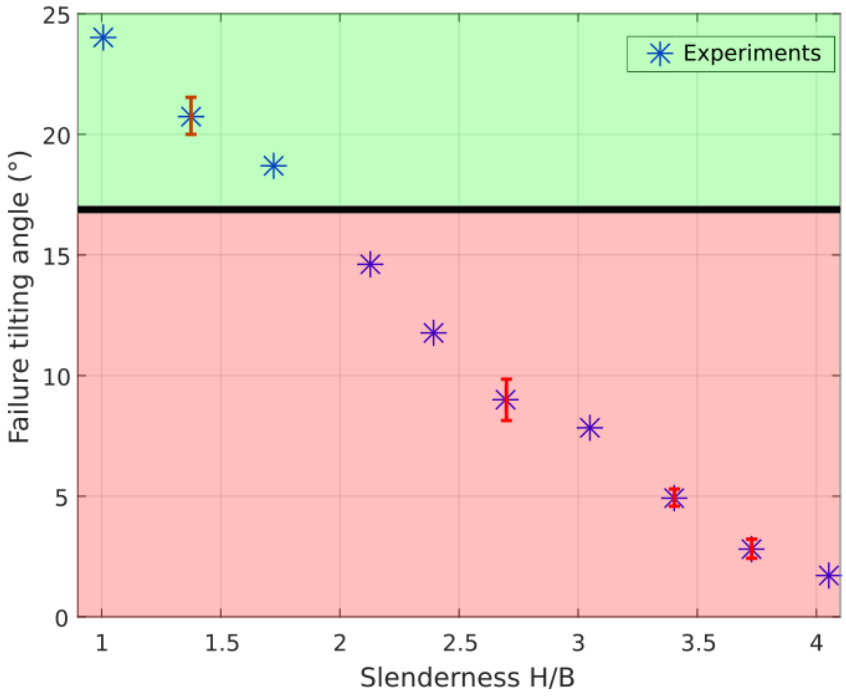


Figure 9: Tilting angle at failure in function of the slenderness of the wall. The more slender walls fell in a toppling mode of failure whereas the less slender fell in a sliding mode of failure.

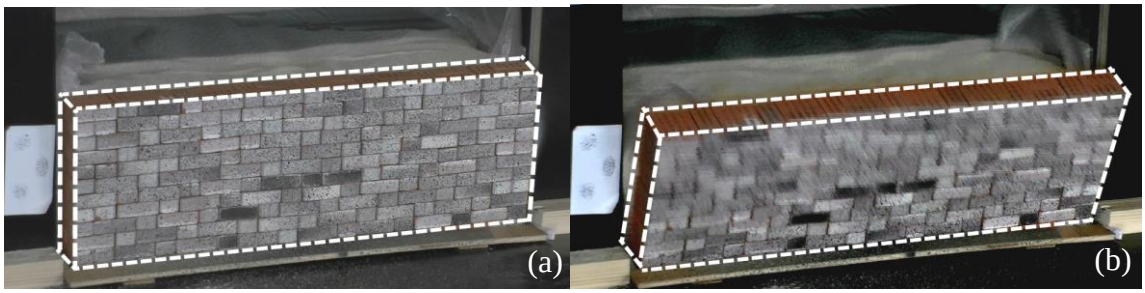


Figure 10: Failure by toppling. (a) Before failure. (b) After failure.

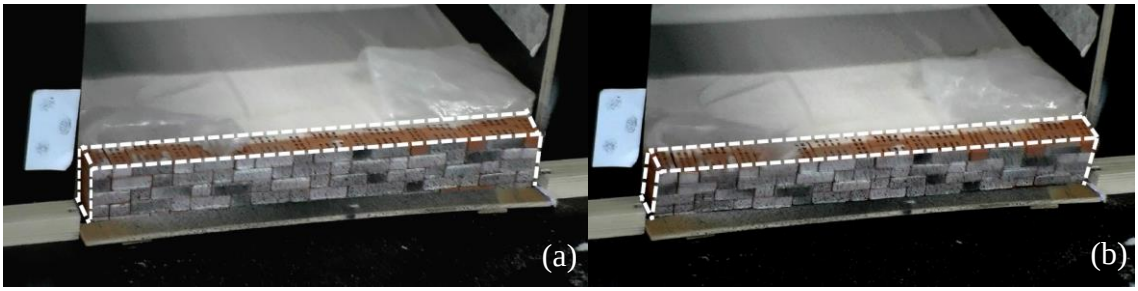


Figure 11: Failure by sliding. (a) Before failure. (b) After failure: the base of the wall is sliding.

Figure 12: Top view of a pattern observed after a failure by overturning. The light color blocks remained stable and the dark color ones have fallen

## 4 NUMERICAL MODELLING

UDEC code (ITASCA [16]) has been used by several authors (among others: [7, 8]) to study the behaviour of slope DSRWs and has been found enough accurate to be used for the study of such systems. Herein, we provide a further validation of this code in the context of pseudo-static studies.

### 4.1 Fundamentals of UDEC

UDEC is a distinct element method used in soil and rock mechanics for solving 3D problems with the statement of plane strain deformations. The dynamic equations of motion are solved by an explicit solution method based on the finite difference method. Discontinuities are easily created between different either rigid or deformable blocks. The interactions between blocks are ruled by a contact's law. Deformable blocks are meshed by an assembly of triangles and the deformation of each zone created is solved by a finite difference method. Laws of continuum mechanics (e.g. Hook's law) are applied to the deformable bodies.

### 4.2 Modelling of the experiments

Because UDEC cannot handle both deformable blocks and rigid blocks in the same computation, the backfill as well as the bricks have been modelled by deformable blocks. Three sub-systems are identified and have to be characterised: the wall, the backfill and the interface between these two sub-systems.

In this work, a Coulomb-slip model is chosen for all contacts existing between bodies. Indeed, it is the simplest model for joints. Moreover, all the parameters required for this model can be easily investigated which is not the case for more sophisticated models. In UDEC, each joint are subdivided in multiple contacts (whose number is linked to the size of the mesh). For each contact, the Coulomb-slip model reads:

$$\Delta\sigma_n = -k_n \times \Delta u_n \quad (1)$$

Where $\Delta\sigma_n$ is the increment of the normal stress, $\Delta u_n$ is the increment of the normal relative displacement between the two blocks in contact and $k_n$ is the normal stiffness of the joint. In the elastic domain, the increment of the tangential stress is ruled by a similar equation:

$$\Delta\tau_s = -k_s \times \Delta u_s \quad (2)$$

Where $\Delta\tau_s$ is the increment of the shear stress, $\Delta u_s$ is the increment of the tangential relative displacement between the two blocks in contact and $k_s$ is the tangential stiffness of the joint. The maximum shear force $\tau_{max}$ is defined in the Coulomb-slip model as:

$$\tau_{max} = C + \sigma_n \times \tan(\Phi) \quad (3)$$

Where C is the cohesion of the joint, $\sigma_n$ the total normal stress and $\Phi$ the friction angle of the contact. C and $\Phi$ are the two main parameters of the Coulomb-slip model. As long as the total shear stress $\tau_s$ is lower than the maximum shear stress $\tau_{max}$, the contact is elastic and Eq. 2 can be used. The shear stress $\tau_s$ is bound to $[-\tau_{max} ; \tau_{max}]$. If the increment of shear stress $\Delta\tau_s$ makes the total stress $\tau_s$ to be out of this range, then $|\tau_s| = |\tau_{max}|$ and the two blocks in contact are sliding. In this model, dilation can be included by modifying the normal relative displacement and correct the normal stress but it will not be used in the modelling of the experiments.

A capture of the used numerical model is presented in Figure 13. The wall is constituted of distinct bricks in contact. The density of bricks was drawn from the experiments and is equal to 1470 kg/m$^3$. The bulk and shear moduli are drawn from a recent similar study [11]. They are set to $K$ = 5.58e8 Pa and $G$ = 4.17e8 Pa. The joints between bricks follow a Coulomb-slip model whose friction angle $\Phi$ is taken equal to 32°. No cohesion was taken into account, since the bricks are dry. Very little dilation was observed by Quezada et al. [11] when using the same bricks. Thus, no dilation was considered in this study. The tangential and normal stiffness ($k_n$ and $k_s$) are both taken equal to 5e12 Pa.m$^{-1}$ as it is commonly done in DEM simulations [7, 9, 11]. In fact, they do not correspond to a physical value but such values allow simulations with faster computational time. They are not too low not to interfere with the quality of results. Each brick was composed of around 100 zones and had seven nodes in contact with the backfill. In fact, in the experiments, each section of the scaled-down walls was different (Figure 5(a)). There were four different sections whose proportions of occurrence are noted in Figure 14. Therefore, the four sections were studied in the numerical modelling. Finally, the first row of bricks (whose translational movement was prevented in the experiments) has not been modelled here. Indeed, it created some discontinuities in the case of a failure by sliding and it has been observed that neither brick of the first layer moved during the experiments.

The backfill has been divided into 5 zones (Figure 13). In the vicinity of the wall, the size of the mesh was very small. As well as we go deeper in the backfill, the size of the mesh increased. It allowed having a good precision of the failure surface in the soil and a good transmission of the mechanical information to the wall without increasing drastically the computation time. Between two successive zones of backfill in contact, the size of the mesh is

divided by two. It avoids the creation of an artificial numerical interface acting as a rigid boundary reflecting waves in the sub-system associated to more refined mesh. The backfill followed a Mohr-Coulomb's constitutive model. The friction is taken equal to 32° and no cohesion was considered. Moreover, as the sand was in a very loose state, no dilation was considered. The average Young's modulus value $E$ is drawn from another numerical work on Hostun sand with a similar low effective pressure which is around 1kPa [11]. The Poisson ratio $\nu = 0.3$ is also drawn from this study. Bulk and shear moduli are deduced from the classical relationships of continuum mechanics knowing $E$ and $\nu$.

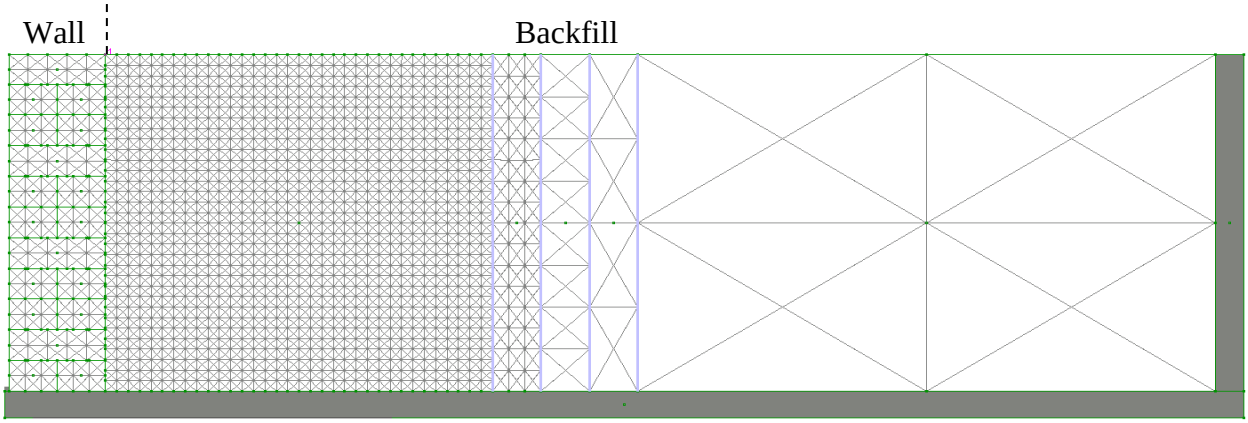


Figure 13: Numerical model of the experiments, different sub-systems with different mesh sizes.

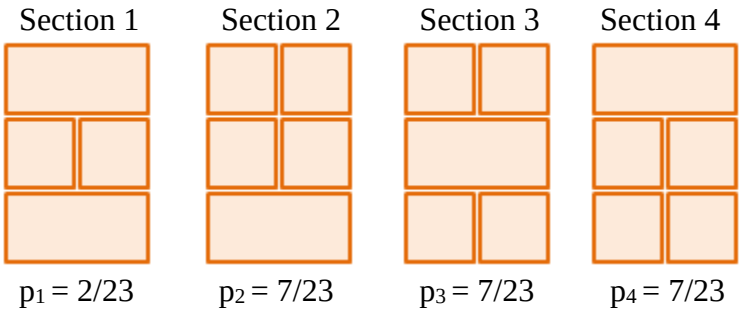


Figure 14: Cross section view of the four different sections observed in the experimental walls.

Last, a Coulomb-slip model is also used for the interface between the bricks and the backfill. As noted before, the friction angle at the interface has been evaluated to 22.7°. No cohesion was considered as the contact is dry. Moreover, since the sand is in a loose state, no dilation is expected. For the sake of simplicity, the tangential and normal stiffness were both taken equal to 1e9 $Pa.m^{-1}$. All the values are gathered in Table 1.

| Property | Wall bricks | Backfill | Interface |
|---|---|---|---|
| ρ ($kg.m^{-3}$) | 1470 | 1310 | |
| K (Pa) | 5.56e8 | 8.33e6 | |
| G (Pa) | 4.17e8 | 3.85e6 | |
| Φ (°) | 32 | 32 | 22.7 |
| Ψ (°) | 0 | 0 | 0 |
| Cohesion (kPa) | 0 | 0 | 0 |
| $k_n$ ($Pa.m^{-1}$) | 1e9 | - | 1e9 |
| $k_s$ ($Pa.m^{-1}$) | 1e9 | - | 1e9 |

Table 1: Mechanical parameters of the numerical model

The procedure used by UDEC to model the experiments is described in the following. Firstly, the wall was erected. Computation cycles were run to reach a stable state. Secondly, the backfill is created and the model reached a stable state under natural gravity. Finally, the gravity is inclined progressively by an increment of 0.1°. The stability of the whole system is checked before incrementing the inclination of the gravity.

The stability criterion is based on energy considerations. The kinetic energy of the wall was computed (through mass and velocities of all nodes). If this energy was small enough, the wall was considered to be stable. If the energy stayed too high during a certain number of cycles, the wall was considered to be at failure and the computation stopped.

As the considered walls did not have the same dimensions, their weight and therefore their kinetic energy varied from one to another. The energy criterion $Ec_{crit}$ of a particular wall (H = 7.8cm and B = 3.4cm) has been calibrated. Then, the other energy criteria were computed following Eq. 4:

$$Ec_{crit}(H) = Ec_{crit}(H = 7.8cm) \times \frac{H}{7.8} \tag{4}$$

To identify the energy criterion $Ec_{crit}$ (7.8), calibrating tests have been conducted. A value of $Ec_{crit}$ (7.8) = 1.0e-10 J has been chosen. When five consecutive stages of 3000 computation cycles led to a kinetic energy lower than $Ec_{crit}$, the wall was considered stable. It was considered unstable when hundred consecutive stages led to a kinetic energy bigger than $Ec_{crit}$. These values have been chosen to ensure that when the computation stopped, the wall was at failure. It means that, letting the computation run for several millions of cycles, the wall collapsed. Moreover, it means that for the inclination just before (inclination at failure minus the increment of 0.1°), the wall was stable even after millions of cycles.

Additionally, as it is commonly done in numerical modelling, a damping is added to force the system to reach an equilibrium state as quickly as possible. The damping used here is a local damping of 0.1. It means that the unbalanced force at a node was artificially reduced by a factor of 0.05 (5% of reduction) which is a small value comparing to classical damping values of 0.7-0.8. This value should be high enough to make the computation faster. But it should be small enough to allow the observation of the failure. Indeed, an excessive value of damping will artificially reduce the kinetic energy of the system and prevent the detection of it.

The ten experimental scaled-down walls have been simulated. For each wall, four tests (according to the four possible sections) have been carried out until failure. Finally, forty simulations have been done and each simulation lasted around 4 hours on a HP computer of 2.3GHz speed.

## 4.3 Validation of the numerical model

### *4.3.1. Prediction of the inclination of gravity*

Four different simulations have been carried out to simulate a given experimental test because four cross section types exist in a single wall (Figure 14). In this case, four different values of inclination of gravity at failure were obtained. A mean value based on the occurrence of each considered section in the experimental walls has been calculated using Eq. 5:

$$\alpha = p_1\alpha_1 + p_2\alpha_2 + p_3\alpha_3 + p_4\alpha_4 \tag{5}$$

Where α is the mean tilting angle and $\alpha_i$ the tilting angle found for the cross section type *i* associated to its occurrence in the experimental wall $p_i$. Finally, using Figure 14, it gives:

$$\alpha = \frac{2\alpha_1 + 7\alpha_2 + 7\alpha_3 + 7\alpha_4}{23} \tag{6}$$

For example, values $\alpha_i$ (i = 1, 2, 3 and 4) for the scaled-down wall of height H = 11.5cm and width B = 3.4cm are respectively equal to 8.0°, 8.0°, 7.1°, 6.2°. The differences observed between the values $\alpha_i$ are on the same range of magnitude than the standard deviation of the experimental tests. It validates therefore the choice of having studied the four different sections instead of a unique one. Then, the tilting angles of the mockup found in the experiments and the weighted one derived from the simulations are compared together (Figure 15). The numerical model gave tilting angles close to those found in the experiments (maximum departure of 18% corresponding to 2.5° and mean departure of 7%).

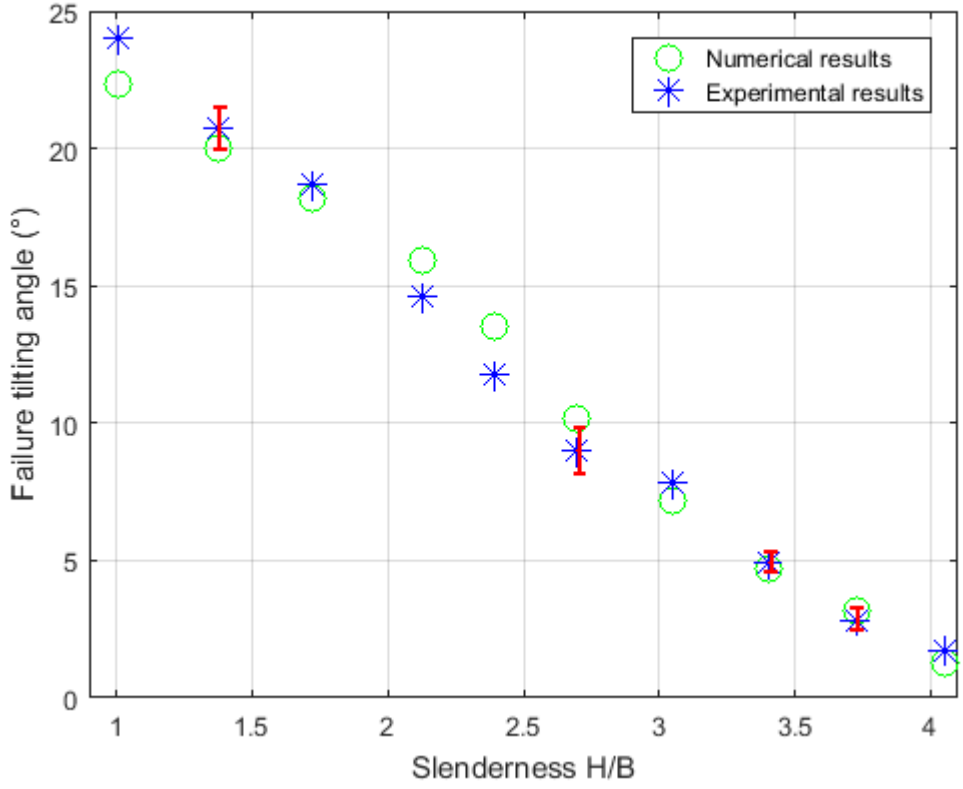


Figure 15: Validation of the numerical model on the basis of the experiments. Error bar in red corresponds to the repeatability tests of experiments (Section 3.1.4).

### *4.3.2. Inclination of the failure surface within the wall*

In addition to the good prediction of the tilting angle at failure, the numerical model appeared to predict very well the mode of failure of the experimental walls. For each wall (and for the four studied sections), the mode of failure was correctly predicted (Figure 16 and 17). Moreover, in the case of a sliding failure, the failure surface (line in the cross-section) crossing the wall has been found systematically horizontal as it was the case in the experiments. In the case of toppling, the numerical failure surface crossing the wall is inclined depending on the studied section: for sections 1 and 2, the failure surface is not inclined because of the header. For sections 3 and 4, the failure surface is inclined compared to the horizontal. A

mean value of the inclination of the failure surface could be computed using the same scheme as Eq. 5. It returned a value of 15° which is close to the failure surface angle that has been evaluated to 11° in the experiments. In addition, we can note that the values of the tilting angle at failure $\alpha_i$ strongly depend on the kind of section in the case of a toppling failure. It confirms the impact of the inclination of the failure surface within the wall (which is strongly related to the geometry of blocks and of their arrangement) on its resistance. Finally, we observed the classical Coulomb's wedge applying a pseudo-static load on the retaining walls. The failure surface in the soil delimiting the wedge is almost straight, which validates the classical statements inherent to the analytical pseudo-static approach (Figure 16 and 17).

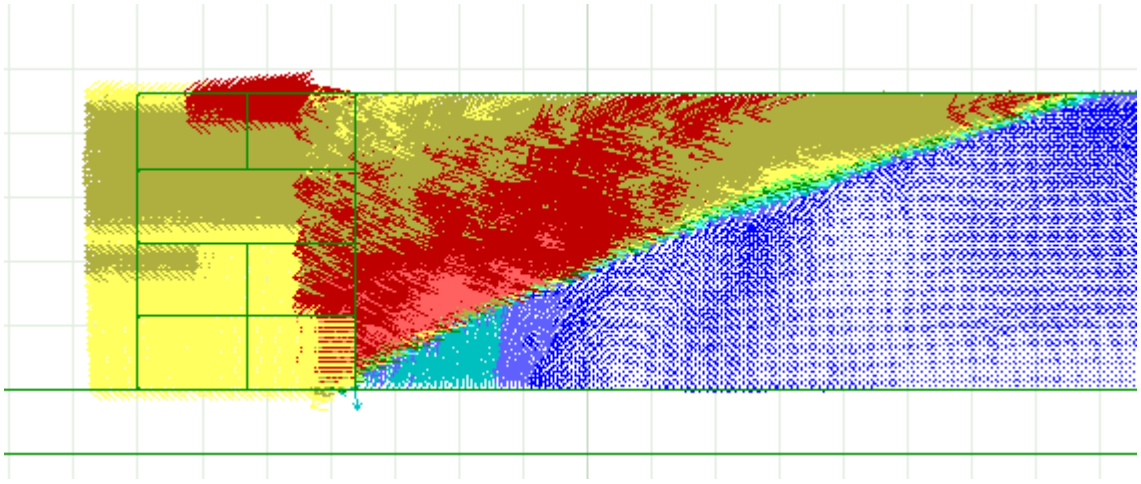

Figure 16: Sliding failure of the wall with the induced Coulomb's wedge at failure; velocity field at the nodes of the meshing.

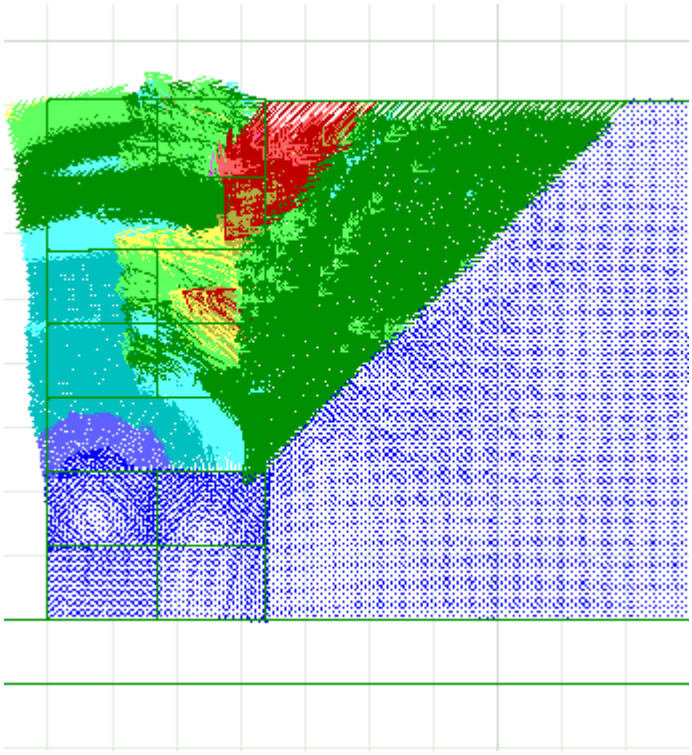

Figure 17: Toppling failure of the wall with the induced Coulomb's wedge at failure; velocity field at the nodes of the meshing.

## 5 CONCLUSIONS AND PERSPECTIVES

Pseudo-static scaled-down experiments have been conducted. A scaled-down mock-up composed of a wall filled by Hostun sand has been tilted until the wall failure. After some calibration experimental tests, the influence of the geometry of the wall on the tilting angle at failure has been studied. It allowed validating the use of a numerical model based on a mixed continuum-discrete approach for the study of the considered problem. Indeed, the simulations performed herein allowed a very good prediction of the tilting angle at failure.

Numerical simulations of the pseudo-static behaviour of DSRWs can be used to complement analytical approaches and to validate them. Indeed, simulations give access to more precise information than it can be done experimentally.

As the pseudo-static approach is known to be over-conservative, dynamic simulations could help to better improve the knowledge of the seismic behaviour of DSRWs. Experiments will have to be carried out to validate the use of the chosen numerical code to model such boundary value problems as performed in this work

## REFERENCES

[1] B. Villemus, J.C. Morel, C. Boutin, Experimental assessment of dry stone retaining wall stability on a rigid foundation, *Engineering Structures*, 29, 2124-2132, 2006.

[2] A.S. Colas, J.C. Morel, D. Garnier, Full-scale field trials to assess drystone retaining wall stability, *Engineering Structures*, 32, 1215-1222, 2010.

[3] C. Mundell, P. McCombie, A. Heath, J. Harkness, Behaviour of drystone retaining structures, *Proceedings of the Institution of Civil Engineers - Structures and Buildings* 163, 3–12, 2010.

[4] L. Alejano, M. Veiga, J. Taboada, M. Dez-Farto, Stability of granite drystone masonry retaining walls: I. analytical design, *Géotechnique*, 62, 1013-1025, 2012 .

[5] L. Alejano, M. Veiga, I. Gomez-Mrquez, J. Taboada, Stability of granite drystone masonry retaining walls: II. relevant parameters and analytical and numerical studies of real walls, *Géotechnique*, 62, 1027-1040, 2012.

[6] H.H. Le, D. Garnier, A.S. Colas, B. Terrade, J.C. Morel, 3D homogenised strength criterion for masonry: Application to drystone retaining walls, *Journal of the Mechanics and Physics of Solids*, 95, 230-253, 2016.

[7] R. Harkness, W. Powrie, X. Zhang, K. Brady, M. O'Reilly, Numerical modelling of full-scale tests on drystone masonry retaining walls, *Géotechnique*, 50, 165–179, 2000.

[8] M. Claxton, R. Hart, P. McCombie, P. Walker, Rigid block distinct element modelling of dry-stone retaining walls in plane strain, *ASCE Journal of Geotechnical and Geoenvironmental Engineering*, 131, 381–389, 2005.

[9] J. J. Oetomo, E. Vincens, F. Dedecker, J. C. Morel, Modeling the 2D behavior of drystone retaining wall by a fully discrete element method, *International Journal for Numerical and Analytical Methods in Geomechanics*, 2015.

[10] C. Mundell, P. McCombie, C. Bailey, A. Heath, P. Walker, Limit equilibrium assessment of drystone retaining structures, *Proceedings of the Institution of Civil Engineers - Geotechnical Engineering*, 162, 203–212, 2009.

[11] J.-C. Quezada, E. Vincens, R. Mouterde, J.-C. Morel, 3d failure of a scale-down dry stone retaining wall : a dem modelling, *Engineering Structures*, 117, 506–517, 2016.

[12] NF EN 1998-5:2005: Design of structures for earthquake resistance - part 5: Foundations, retaining structures and geotechnical aspects, Association Française de Normalisation (AFNOR - French standard institute), 2005.

[13] S. Okabe, General theory of earth pressure, *Journal of the Japanese Society of Civil Engineers*, 12, 1926.

[14] N. Mononobe, H. Matsuo, On the determination of earth pressures during earthquakes, *World Engineering Conference*, 9, p.176, 1929.

[15] H. S. M. H. Baziar, M. R. Moghadam, Sliding stability analysis of gravity retaining walls using the pseudo-dynamic method, *Geotechnical Engineering*, 166, 389–398, 2013.

[16] Itasca Consulting Group Inc. *Universal Distinct Element Code (UDEC) Version 2.0: user's manual*, Minneapolis, Minnesota, 2th ed. 1993.

[17] J. D. E. Flavigny, B. Palayer, Note technique-le sable d'hostun, *Revue française de géotechnique*, 67–70, 1990.